

Article

Constrained Integrated Guidance and Control Scheme for Strap-Down Hypersonic Flight Vehicles with Partial Measurement and Unmatched Uncertainties

Minzhou Dong *, Xinkai Xu and Feng Xie

School of Astronautics, Northwestern Polytechnical University, Xi'an 710072, China

* Correspondence: dongminzhou_nwpu@163.com

Abstract: This paper investigates the issue of integrated guidance and control (IGC) design for strap-down hypersonic flight vehicles with partial measurement information and unmatched uncertainties. A constrained IGC scheme is proposed by combining the barrier Lyapunov function-based backstepping methodology and the specific output-based finite-time disturbance observer. Different from the existing methods, which require the state information and matched disturbances, the main features of the presented approach is capable of addressing the partial measurement knowledge and unmatched uncertainties simultaneously. The IGC model of hypersonic flight vehicles is first formulated, and based on that, the specific output-based finite-time disturbance observer (OFTDO) is proposed to achieve the finite-time estimation of the unmatched uncertainties through the output. Then, the constrained IGC strategy is constructed via the backstepping technique. The stability of the closed-loop system including the estimation and tracking errors dynamics is analyzed in detail. The effectiveness of the proposed method is verified by numerical simulations and Monte-Carlo tests.

Keywords: integrated guidance and control; partial measurement; disturbance observer; unmatched uncertainties; strap-down hypersonic flight vehicles



Citation: Dong, M.; Xu, X.; Xie, F. Constrained Integrated Guidance and Control Scheme for Strap-Down Hypersonic Flight Vehicles with Partial Measurement and Unmatched Uncertainties. *Aerospace* **2022**, *9*, 840. <https://doi.org/10.3390/aerospace9120840>

Academic Editor: Maolong Lv

Received: 30 September 2022

Accepted: 14 December 2022

Published: 17 December 2022

Publisher's Note: MDPI stays neutral with regard to jurisdictional claims in published maps and institutional affiliations.



Copyright: © 2022 by the authors. Licensee MDPI, Basel, Switzerland. This article is an open access article distributed under the terms and conditions of the Creative Commons Attribution (CC BY) license (<https://creativecommons.org/licenses/by/4.0/>).

1. Introduction

Much research on hypersonic flight vehicles (HFV) has been conducted for a long time in both military and civil fields [1–3]. The significant merits over the traditional flight vehicles are provided in many fields, such as the near-space accessibility at affordable costs [4–7]. In particular, the strap-down HFV is capable of sufficiently decreasing the cost due to the equipment of the strap-down seeker and has attracted much attention [8,9]. The attitude control of the strap-down HFV has been researched extensively; however, the integrated guidance and control (IGC) issue is still challenging since it plays an important role in the mission completion [10]. Different from the attitude or guidance law, the IGC scheme combines both systems and is capable of achieving a small miss distance. In particular, the separation principle of attitude and guidance systems is no longer satisfied for the HFV in the large envelope flight, and thus the IGC method can consider both systems in an integrated manner and guarantee the success of the mission.

In the IGC design, many methods have been proposed to cope over the past decades. Some classical control strategies, including backstepping control [10], sliding mode control [11,12] and model predictive control [13], have been employed for IGC designs. In these methods, the backstepping approach can deal with the IGC model due to the structure of the IGC model and has been investigated in many articles. The sliding mode control can achieve strong robustness due to the unchanged condition during the sliding mode surface. The IGC method has been surveyed in [14]. Unfortunately, these methods cannot deal with the constraint issue for the strap-down hypersonic flight vehicles. This type of HFV has a low-cost strap-down seeker, which causes field-of-view (FOV) limitation. Once the limitation is violated, the target will be missed in the view and the mission of the HFV will

fail. Hence, the IGC design for the strap-down HFV should consider the FOV constraint carefully. However, few articles focus on this issue, especially with the consideration of the unmatched uncertainties and partial measurement. Recently, the barrier function-based constrained control method has been developed to effectively address the constrained issue [15–18], and has been applied in many engineering cases [19–21]. Thanks to this technique, we can consider and introduce it into the IGC law design to deal with the FOV constraint.

The disturbance observer (DO) technique has attracted much attention in the research field since it has strong ability in the enhancement of the robustness for the nominal controller. The disturbance observer is capable of effectively estimating and canceling out the matched and unmatched disturbances so as to obtain better disturbance rejection performance. Moreover, it provides a framework for the control design to involve the classical control, such as PID, dynamic inverse control and the backstepping method, to successfully enhance their robustness and construct a DO-based control version. The DO was proposed in [22] for the first time, and has been applied in the industrial examples in the time domain and frequency domain. The unknown input observer is a representative version of the linear DO and the nonlinear version was proposed in [23]. The extended state observer is a part of the active disturbance rejection control and can achieve the fine estimation of the uncertainties [24]. An overview of the disturbance observer technique can be found in [25]. Recently, the disturbance observer has been developed for the function-constrained disturbance, which further extended and relaxed the requirement of the uncertainties. The DO technique has been applied to the attitude control of hypersonic flight vehicles [3,5] and guidance system design [12]. In particular, the integrated guidance and control system [26] has also been researched by virtue of the DO method to combine with the sliding mode control and backstepping control [27,28]. However, the above DO requires that the state is completely measured, which is not always satisfied in the engineering. For the strap-down hypersonic flight vehicles, the strap-down seeker is equipped fixed with the body of the vehicles, and the sensors are usually used to measure the body line-of-sight angle. The complete states may not be measured for the aim of low cost. Thus, there only exists partial information in the IGC model, which makes the use of the existing DO methods difficult.

To address the issues above, this paper proposes the specific output-based finite-time disturbance observer to achieve the finite-time estimation of the unmatched uncertainties through the output, and presents a constrained IGC law for the FOV limitations. The main features of this paper are listed as follows:

- (1) Considering the partial information and unmatched uncertainties in the IGC model, the paper proposes a novel output-based finite-time disturbance observer to achieve the finite-time estimation of the unmatched uncertainties through the output. The detailed algorithm and the stability of the disturbance observer are also provided.
- (2) The constrained IGC law is presented to achieve the satisfaction of the FOV limitation, which ensures the body line-of-sight angle inside the constrain and guarantees the success of the mission of the hypersonic flight vehicles. The stability analysis of the closed-loop system is carried out in detail.

The remainder of the paper is organized as follows. Section 2 lays down the problem formulation and some key issues. The out-based finite-time disturbance observer is designed in Section 3, and Section 4 presents the main results in the IGC law and the stability analysis. Section 5 illustrates simulation studies to verify the proposed control approach. The paper concludes in Section 6.

2. Problem Statement

2.1. Integrated Guidance and Control Dynamics for Strap-Down Hypersonic Flight Vehicles

Consider the geometry of a planer interception depicted in Figure 1, where (X_I, Z_I) denotes the inertial reference frame. The longitudinal dynamics of the integrated guidance and control system for strap-down missiles can be represented as: [12]

$$\begin{aligned} \dot{R} &= V_T \cos(q - \theta_T) - V_M \cos(q - \theta_M) \\ R\dot{q} &= -V_T \sin(q - \theta_T) + V_M \sin(q - \theta_M) \\ \dot{\alpha} &= w_z + \frac{-Y + mg \cos \theta_M}{mV_M} \\ \dot{w}_z &= \frac{M_z}{J_z} \end{aligned} \tag{1}$$

where R is the relative distance between a maneuver target and the missile, q is the angle of line-of-sight (LOS), and α, w_z represent the angle of attack and the pitch rate, respectively. The velocities of the missile and the target V_M and V_T are assumed to be constant. The terms θ_M and θ_T are their flight path angles. Additionally, m denotes the mass of the missile, and J_z is the moment of inertia around the z -axis.

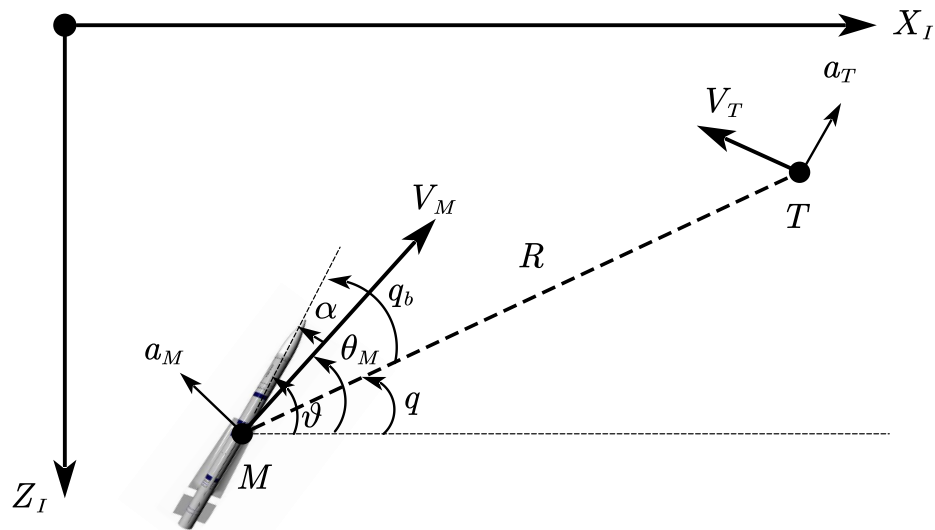


Figure 1. Longitudinal missile–target engagement geometry.

The aerodynamic lift force Y and moment M_z are approximated as follows:

$$\begin{aligned} Y &= 57.3QS(c_y^\alpha \alpha + c_y^{\delta_z} \delta_z) \\ M_z &= 57.3QSL(m_z^\alpha \alpha + \frac{L}{57.3V_M} m_z^{w_z} w_z + m_z^{\delta_z} \delta_z) \end{aligned} \tag{2}$$

where $Q = \frac{1}{2}\rho V_M^2$ is the dynamic pressure with the air density ρ , and δ_z represents the elevator deflection. The terms S and L are the reference area and reference length, respectively, and $c_y^\alpha, c_y^\delta, m_z^\alpha, m_z^{w_z}, m_z^{\delta_z}$ represent aerodynamic coefficients, which are set as:

$$\begin{aligned} a_1 &= \frac{57.3QSc_y^\alpha}{mV_M}, \quad a_2 = \frac{57.3QSc_y^{\delta_z}}{mV_M}, \quad a_3 = \frac{57.3QSLm_z^\alpha}{J_z} \\ a_4 &= \frac{57.3QSL^2 m_z^{w_z}}{J_z V_M}, \quad b = \frac{57.3QSLm_z^{\delta_z}}{J_z} \end{aligned} \tag{3}$$

Taking the derivative and combining (1) yield that:

$$2\dot{R}\dot{q} + R\ddot{q} = -\dot{V}_T \sin(q - \theta_T) + \dot{V}_M \sin(q - \theta_M) + a_T \cos(q - \theta_T) - a_M \cos(q - \theta_M) \quad (4)$$

where $a_M = V_M \dot{\theta}_M$ and a_T represent the accelerations of the hypersonic flight vehicle and the target, respectively. In this paper, the target is assumed to be stationary, which leads to $\dot{V}_T = 0$ and $a_T = 0$. Then, (4) can be rewritten as:

$$2\dot{R}\dot{q} + R\ddot{q} = -a_M \cos(q - \theta_M) + \dot{V}_M \sin(q - \theta_M) \quad (5)$$

Let $V_q = R\dot{q}$; then, according to (5) one has that:

$$\dot{V}_q = -\frac{\dot{R}}{R}V_q - a_M \cos(q - \theta_M) + \dot{V}_M \sin(q - \theta_M) \quad (6)$$

Consider the relationships $\alpha = \vartheta - \theta_M$ and $\dot{\vartheta} = w_z$, where ϑ denotes the pitch angle of the hypersonic flight vehicle. Define that $x_1 = \frac{V_q}{-57.3QSc_y^\alpha}$, $x_2 = \alpha$, $x_3 = w_z + \frac{g \cos \theta_M}{V_M}$, $u = \delta_z$, $b = \frac{57.3QSLm_z^{\delta_z}}{J_z}$; then models (1) and (2) can be rewritten as:

$$\begin{aligned} \dot{x}_1 &= x_2 + d_1 \\ \dot{x}_2 &= x_3 \\ \dot{x}_3 &= a_3 x_2 + a_4 x_3 + bu + d_3 \end{aligned} \quad (7)$$

where:

$$\begin{aligned} a_3 &= \frac{57.3QSLm_z^\alpha}{J_z}, \quad a_4 = \frac{QSL^2 m_z^{w_z}}{J_z V_M} \\ d_1 &= -\frac{\dot{R}}{R}x_1 + \frac{g \cos \theta_M \cos(q - \theta_M)}{-57.3QSc_y^\alpha / m} - x_2[1 - \cos(q - \theta_M)] + \dot{V}_M \sin(q - \theta_M) + w_1 \\ d_3 &= \frac{d(\frac{\cos(\theta_M)}{V_M})}{dt} - a_4 \frac{g \cos \theta_M}{V_M} + w_3 \end{aligned} \quad (8)$$

where a_3 and a_4 represent the simplified aerodynamic coefficients, d_1 and d_3 denote the time-varying unmatched uncertainties, and w_1 and w_3 denote the time-varying perturbations caused by variations of aerodynamics parameters. In this paper, there are several focuses in the IGC model, which causes the difficulties in designing the IGC law for the strap-down hypersonic vehicles, which are analyzed in detail in the following subsections.

2.2. Field-of-View Constraint

Due to the use of the strap-down seeker in the hypersonic vehicles, there exists the hard limitation in the body line-of-sight (BLOS), which is represented by q_b , which is denoted as the angle between the axis of the body and the line of the vehicle-target. In fact, the FOV constraint is little considered for the flight vehicles with the platform seeker. Since the platform has a gimbal structure, it can provide a wide FOV range. However, for the hypersonic vehicles equipped with a strap-down seeker, the detective range depends on the FOV. Once the FOV is escaped, the target will be missed and result in mission failure.

For the strap-down hypersonic vehicle, the optical axis of the seeker is connected fixedly with the vehicle's body, and the BLOS angle q_B should be strictly limited in the range of the seeker's effective field of view, which can be represented as $q_{b\min} \leq q_b \leq q_{b\max}$, where $q_{b\min}$ and $q_{b\max}$ denote the lower and upper limitations of the BLOS, respectively. During the final phase of the engagement, the BLOS constraint should always be met, and its representation is obtained by the following relationship:

$$\begin{aligned} q_b &= q - \vartheta \\ \dot{q}_b &= \dot{q} - \omega_z \end{aligned} \quad (9)$$

In this paper, to simplify the researched issue, the FOV constraint is set as a symmetric form, which can be expressed as:

$$|q_b| \leq Q_c \quad (10)$$

where k_c is a positive constant.

Define that $x_0 = q_b$; then, we have that $\dot{x}_0 = a_0 x_1 + d_0$, where $a_0 = -\frac{57.3 Q S c_y^\alpha}{R}$, $d_0 = -\omega_z$. Thus, the IGC model is updated as the following expression:

$$\begin{aligned} \dot{x}_0 &= x_1 + d_0 \\ \dot{x}_1 &= x_2 + d_1 \\ \dot{x}_2 &= x_3 \\ \dot{x}_3 &= a_3 x_2 + a_4 x_3 + bu + d_3 \end{aligned} \quad (11)$$

2.3. Issues of Unmatched Uncertainties and Partial Measurement

As demonstrated in model (11), the IGC model for strap-down hypersonic vehicles is obtained, which exhibits the following two features.

As seen in (11), the IGC model is formulated as a model with the unmatched uncertainties d_0, d_1, d_2, d_3 . The uncertainties d_0, d_1 do not occur in the control channel and thus cannot be dealt with using the traditional control methods. These unmatched uncertainties will cause steady-state errors in the tracking control and even result in the instability and large miss distance of the whole guidance and control system.

On the other hand, the model information may be not completely known. Generally, the state information is obtained through the measurement by the sensors. However, for several types of flight vehicles, some state measurements may be not available. Thus, differently from the general hypersonic vehicles, the output of the whole IGC model is set as $y = [x_0, x_1, x_2]^T$, and the controller should be designed under the output measurement.

2.4. Control Objective

In this paper, the control goal of the integrated guidance and control system is to design an IGC law δ_z to ensure the success of the interception under the partial measurement and unmatched uncertainties d_0, d_1, d_3 . Moreover, the FOV constraint $|q_b = x_0| \leq Q_c$ is always guaranteed in the overall flight envelope.

3. Output-Based Finite-Time Disturbance Observer

The important task for addressing the control goal is to deal with the unmatched uncertainties issue by using the partial measurement information. The disturbance observer is a type of estimator used to obtain the disturbance observation, which is capable of solving the problem of the unmatched uncertainties. However, the existing disturbance observers usually estimate the uncertainties using the complete state information, and it is difficult for them to obtain the unmatched uncertainties only by virtue of the output. Therefore, in this part, we first propose a novel output-based finite-time disturbance observer (OFTDO), which not only estimates the unmatched uncertainties precisely, but also can achieve the finite-time convergence of the estimate errors.

Consider an uncertain system:

$$\begin{cases} \dot{x} = Ax + Bu + Gd \\ y = Cx \end{cases} \quad (12)$$

where $x \in \mathbb{R}^n, u \in \mathbb{R}^m, y \in \mathbb{R}^p$ denote the state, input and output, respectively, and $d \in \mathbb{R}^q (q \leq n)$ is the lump disturbance. Matrices A, B, C, G have proper dimensions. First of all, some necessary assumptions are listed below.

Assumption 1. The system (12) is controllable and strongly observable.

Assumption 2. The matrix G has a column full rank.

Assumption 3. The disturbance d and its derivatives up to order r are bounded, where r is a known constant greater than zero.

Remark 1. The strongly observability in Assumption 1 means that $y = Cx \equiv 0$ implies that $x \equiv 0$ on every nondegenerate interval $[t_1, t_2]$ ($t_1 < t_2$) and for every piecewise continuous (or integrable) function (control) $u(t)$ on $[t_1, t_2]$. It is a necessary condition to construct the state and uncertainties estimates in this paper. More details can be found in [29].

Note that the standard DOs require the complete knowledge of the states when the unmatched uncertainties exist, and thus they are not suitable for the IGC system in this paper where the partial measurement and unmatched uncertainties are considered. Therefore, in the following part a novel OFTDO is presented to estimate the disturbance precisely via the system output.

Theorem 1. For System (12), if Assumptions 1–3 are satisfied, and the proposed OFTDO is designed as:

$$\begin{cases} \dot{z} = Az + Bu + L(y - Cz) \\ \hat{x} = \sigma_{\kappa-1} + z \\ \hat{d} = (G^T G)^{-1} G^T (\sigma_{\kappa} - \bar{A} \mathbf{1} \sigma_{\kappa-1}) \\ \dot{\sigma}_0 = k_0 L_p^{\frac{1}{\ell+1}} \Phi^{\frac{\ell}{\ell+1}} (\sigma_0 - H) + \sigma_1 \\ \dot{\sigma}_j = k_j L_p^{\frac{1}{\ell+1-j}} \Phi^{\frac{\ell-j}{\ell+1-j}} (\sigma_j - \dot{\sigma}_{j-1}) + \sigma_{j+1} \\ \dot{\sigma}_{\ell} = k_{\ell} L_p \text{sgn}(\sigma_{\ell} - \dot{\sigma}_{\ell-1}) \end{cases} \quad (13)$$

where $\ell = r + \kappa - 2$ is the differentiator order, and the gain $k_j (j = 1, \dots, \ell - 1)$ can be obtained as in [30]. The matrix L is selected such that $A - LC$ is Hurwitz. The function $\Phi^a(v) = [|v_1|^a \text{sgn}(v_1), \dots, |v_n|^a \text{sgn}(v_n)]^T$ for a vector $v = [v_1, \dots, v_n]^T$ and a constant $a > 0$. The vector $H = M_{\kappa}^+ \begin{bmatrix} J_{\kappa-1} & \mathbf{0} \\ \mathbf{0} & I \end{bmatrix} Y$ where $Y = [y_e^T, \dots, (y_e^{[\kappa-1]})^T]^T$. Herein, $y_e = C(x - z)$ and $y_e^{[i]}$ represent the i th anti-differentiator of y_e , i.e., $y_e^{[i]} = \int_0^t \dots \int_0^t y_e d\tau_i \dots dt$. The matrices M_{κ} and $J_{\kappa-1}$ are constructed in the proof. The parameter L_p is the Lipschitz constant of Y^{ℓ} . Then, the estimation \hat{x} and \hat{d} will converge to the actual values in finite time.

Proof. The proof is shown in the following three steps.

(1) Define that $e = x - z$ and one has $\dot{e} = \dot{x} - \dot{z} = (A - LC)e + Gd$. Therefore, the following error dynamics are obtained:

$$\begin{cases} \dot{e} = \bar{A}e + Gd \\ y_e = Ce \end{cases} \quad (14)$$

where the matrix $\bar{A} = A - LC$ is Hurwitz.

(2) Let $M_1 = C$ and $J_1 = (M_1 G)^{\perp}$. Herein, the symbol \perp is defined as follows. For a matrix $K \in \mathbb{R}^{n \times m}$ with $\text{rank}(K) = q$, the matrix $K^{\perp} \in \mathbb{R}^{(n-r) \times n}$ with $\text{rank}(K) = n - q$ is defined such that $K^{\perp} K = 0$.

The matrix M_{κ} can be defined in a recursive way as follows:

$$\begin{aligned} M_{\kappa} &= \begin{bmatrix} (M_{\kappa-1} G)^{\perp} M_{\kappa-1} \bar{A} \\ M_1 \end{bmatrix} \\ J_{\kappa-1} &= (M_{\kappa-1} G)^{\perp} \begin{bmatrix} J_{\kappa-2} & \mathbf{0} \\ \mathbf{0} & I \end{bmatrix} \end{aligned} \quad (15)$$

If the system is strongly observable, there exists a unique positive integer $\kappa \leq n$ such that the matrix M_κ satisfies the relationship $rank(M_\kappa) = n$ [31,32]. Therefore, the following expression can be obtained:

$$M_\kappa e = \frac{d^{\kappa-1}}{dt^{\kappa-1}} \begin{bmatrix} J_{\kappa-1} & \mathbf{0} \\ \mathbf{0} & I \end{bmatrix} \begin{bmatrix} y_e \\ \vdots \\ y_e^{[\kappa-1]} \end{bmatrix} = \frac{d^{\kappa-1}}{dt^{\kappa-1}} \begin{bmatrix} J_{\kappa-1} & \mathbf{0} \\ \mathbf{0} & I \end{bmatrix} Y \tag{16}$$

where $y_e^{[i]}$ represents the i th anti-differentiator of y_e , i.e., $y_e^{[i]} = \int_0^t \dots \int_0^t y_e d\tau_i \dots dt$. Note that $H = M_\kappa^+ \begin{bmatrix} J_{\kappa-1} & \mathbf{0} \\ \mathbf{0} & I \end{bmatrix} Y$, and thus, we can obtain that $e = \frac{d^{\kappa-1}}{dt^{\kappa-1}} H$.

(3) Using the high-order sliding mode (HOSM) differentiator

$$\begin{cases} \dot{\sigma}_0 = k_0 L^{\frac{1}{\ell+1}} \Phi^{\frac{\ell}{\ell+1}}(\sigma_0 - H) + \sigma_1 \\ \dot{\sigma}_j = k_j L^{\frac{1}{\ell+1-j}} \Phi^{\frac{\ell-j}{\ell+1-j}}(\sigma_j - \dot{\sigma}_{j-1}) + \sigma_{j+1} \\ \dot{\sigma}_\ell = k_\ell L \text{sgn}(\sigma_\ell - \dot{\sigma}_{\ell-1}) \end{cases} \tag{17}$$

to estimate the vector H , the variable e can be obtained. It is proven that with the proper choice of the constants k_j , the equality $\sigma_j = \frac{d^j}{dt^j} H$ is satisfied after a finite time [30]. Hence, we have that $e = \sigma_{\kappa-1}$, and $\hat{x} = \sigma_{\kappa-1} + z$ holds after a certain time. Moreover, for the error dynamics (14), we have $e = \sigma_{\kappa-1}$, $\dot{e} = \sigma_\kappa$, and thus

$$\hat{d} = (G^T G)^{-1} G^T (\sigma_\kappa - \bar{A} \sigma_{\kappa-1}) \tag{18}$$

can be obtained. The proof is completed. \square

The schematic diagram of the proposed OFTDO algorithm is provided in Figure 2. As shown in Figure 2, the presented estimation approach achieves a finite-time observation for the unmatched by introducing a sliding mode technique when only partial information can be measurable.

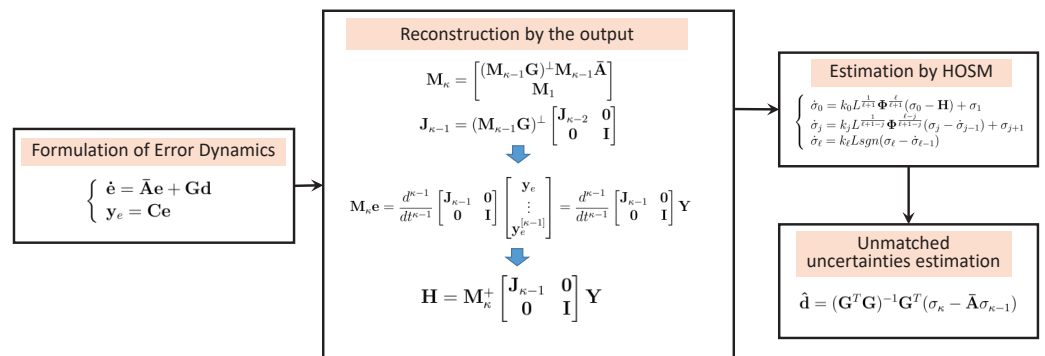


Figure 2. Schematic diagram of the proposed OFTDO.

Remark 2. The high-order sliding mode differentiator differentiates a continuous signal and obtain its derivative up to r . Assumption 3 is necessary for the introduction of the HOSM technique. Moreover, the HOSM method is capable of ensuring the continuousness of the control signal since the sign function is hidden in the integral part, rather than introducing the discontinuous term in the control in the standard sliding mode control.

4. Constrained IGC Scheme Design

As shown in the context above, the predefined requirement on the BLOS constraint is $|q_b| < Q_c$, and the designed constrained IGC scheme should ensure that the state converges to the origin and the BLOS is always inside the prescribed limitations. First, some necessary lemmas are given to facilitate the control design and stability analysis.

4.1. Preliminaries

Lemma 1 ([15]). For any positive constants \underline{k}, \bar{k} , let $Z = z \in \mathbb{R} : -\underline{k} < z < \bar{k} \subset \mathbb{R}$ and $N = \mathbb{R}^l \times Z \subset \mathbb{R}^{l+1}$ are an open set. Consider the system:

$$\dot{\eta} = h(t, \eta) \tag{19}$$

where $\eta = [\omega, z]^T \in N$, $h : \mathbb{R}_+ \times N \rightarrow \mathbb{R}^{l+1}$ is piecewise continuous in t , and locally Lipschitz in h , uniformly in t , on $\mathbb{R}_+ \times N$. Suppose that there exist positive definite functions $U : \mathbb{R}^l \rightarrow \mathbb{R}_+$ and $V_1 : Z \rightarrow \mathbb{R}_+$, both of which are continuously differentiable in their respective domains, such that $V_1 \rightarrow \infty$ as $z \rightarrow -\underline{k}$ or $z \rightarrow \bar{k}$. Let $V(\eta) = V_1(z) + U(\omega)$, and $z(0) \in (-\underline{k}, \bar{k})$, if the inequality

$$\dot{V} = \frac{\partial V}{\partial \eta} h \leq 0 \tag{20}$$

holds in the set $z \in (-\underline{k}, \bar{k})$, then $z \in (-\underline{k}, \bar{k})$ for all $t \geq 0$.

Lemma 2 ([16]). For any positive constant A , the following inequality holds for all z in the interval $|z| < A$:

$$\log\left(\frac{A^{2p}}{A^{2p} - z^{2p}}\right) < \frac{z^{2p}}{A^{2p} - z^{2p}} \tag{21}$$

where p is a positive constant.

Lemma 3 ([19]). For any $\delta > 0$ and $\eta \in \mathbb{R}$, the following inequality always holds:

$$0 \leq |\eta| - \eta \tanh\left(\frac{\eta}{\delta}\right) \leq k_p \delta, \quad k_p = 0.2785 \tag{22}$$

Remark 3. Lemma 1 provides the fundamental theory for guaranteeing the stability of the system with a state constraint. In other words, the constraint issue has been solved through the establishment of the proper Lyapunov function. Lemma 2 gives an important inequality for the stability analysis.

4.2. OFTDO Design

For the application in the IGC system (11), the following assumption is given for the design of the OFTDO.

Assumption 4. The lump uncertainties $d_i (i = 0, 1, 3)$ their its first and second derivatives are bounded.

Remark 4. Note that only the aerodynamic perturbations are considered, and thus the wind gusts are not involved in the paper. In (8), the unmatched uncertainties are functions of the states, and thus d_0, d_1, d_3 and their first- and second-order derivatives can be considered to be bounded in the flight. Therefore, Assumption 4 is reasonable.

First, it can be checked and confirmed that Assumptions 1 and 2 are satisfied.

For the IGC model (11), it can be obtained that $C = \begin{bmatrix} 1 & 0 & 0 & 0 \\ 0 & 1 & 0 & 0 \\ 0 & 0 & 1 & 0 \end{bmatrix}$, $B = \begin{bmatrix} 0 \\ 0 \\ 0 \\ b \end{bmatrix}$, and

$G = \begin{bmatrix} 0 & 1 & 0 \\ 0 & 0 & 1 \\ 0 & 0 & 0 \\ b & 0 & 0 \end{bmatrix}$. The disturbance is reconstructed by $d = \left[\frac{d_3}{b} \quad d_0 \quad d_1\right]^T$ to adapt the

use of Theorem 1. Then, it can be verified that the system is strongly observable according to [29].

Then, following (15), it can be calculated that $M_1G = CG = \begin{bmatrix} 0 & 1 & 0 \\ 0 & 0 & 1 \\ 0 & 0 & 0 \end{bmatrix}$, thus $J_1 =$

$(M_1G)^\perp = [0 \quad 0 \quad 1]$. If the matrix L is set as $L = l_{ij}(i = 1, 2, 3, 4; j = 1, 2, 3, 4)$, thus

$\bar{A} = A - LC = \begin{bmatrix} -l_{11} & 1 - l_{12} & -l_{13} & 0 \\ -l_{21} & -l_{22} & 1 - l_{23} & 0 \\ -l_{31} & -l_{32} & -l_{33} & 1 \\ -l_{41} & -l_{42} & a_3 - l_{43} & a_4 \end{bmatrix}$. Then, it follows that

$$M_2 = \begin{bmatrix} (M_1G)^\perp M_1 \bar{A} \\ M_1 \end{bmatrix} = \begin{bmatrix} -l_{31} & -l_{32} & -l_{33} & 1 \\ 1 & 0 & 0 & 0 \\ 0 & 1 & 0 & 0 \\ 0 & 0 & 1 & 0 \end{bmatrix}, \tag{23}$$

which is a column full rank, and thus $\kappa = 2$.

According to Assumption 4, it can be found that Assumption 3 means that $r = 2$, and thus we have that $\ell = r + \kappa - 2 = 2$. Therefore, the following HOSM differentiator:

$$\begin{cases} \dot{\sigma}_0 = -k_1 \Phi^{\frac{1}{3}}(\sigma_0 - H) + \sigma_1 \\ \dot{\sigma}_1 = -k_1 \Phi^{\frac{1}{2}}(\sigma_1 - \dot{\sigma}_0) + \sigma_2 \\ \dot{\sigma}_2 = -k_2 \text{sgn}(\sigma_2 - \dot{\sigma}_1) \end{cases} \tag{24}$$

is used to estimate the variable $Y = [y_e, \int_0^t y_e d\tau]^T$, where the output error $y_e = [x_0, x_1, x_2]^T$. Then, the estimate of d is obtained by $\hat{d} = (G^T G)^{-1} G^T (\sigma_2 - \bar{A} \sigma_1)$. Note that the sign function will cause some unnecessary oscillation in the control input, and thus we instead use the saturation function to replace it in the simulation.

4.3. Constrained IGC Law Design

In the procedure of IGC law design, the backstepping technique is used. We define the tracking error as $e_0 = x_0 - x_{0,d}$ where $x_{0,d}$ denotes the desired reference. In this paper, the reference is set as $x_{0,d} = 0$. Then, one has that:

$$\dot{e}_0 = \dot{x}_0 - \dot{x}_{0,d} = x_1 + d_0 \tag{25}$$

We introduce the virtual control $x_{1,d}$, which is designed as:

$$x_{1,d} = -k_0 e_0 - \frac{e_0}{2(Q_c^2 - e_0^2)} - \hat{d}_0 \tag{26}$$

where the term \hat{d}_0 is the estimation from the proposed OFTDO and k_0 is a positive constant. Then, substituting (26) into (25) yields:

$$\dot{e}_0 = -k_0 e_0 + x_1 - x_{1,d} - \frac{e_0}{2(Q_c^2 - e_0^2)} + \tilde{d}_0 \tag{27}$$

where $\tilde{d}_0 = d_0 - \hat{d}_0$ represents the estimation of the uncertainties.

To avoid the “explosion of terms” problem, the dynamic surface technique is applied, and the following filter is presented in this paper:

$$\dot{x}_{1,c} = -\frac{x_{1,c} - x_{1,d}}{\tau_1} - \zeta_1 \tanh(c_1(x_{1,c} - x_{1,d})), \quad x_{1,c}(0) = x_{1,d}(0) \tag{28}$$

where ζ_1, c_1, τ_1 are positive constants. The hyperbolic tangent function term $\zeta_1 \tanh(c_1(x_{1,c} - x_{1,d}))$ is a typical nonlinear function that is capable of accelerating the convergence when the filter errors are far away from zero and avoiding the chattering around zero. Consequently, the performance of the filter can be effectively improved compared with the standard first-order filter.

Next, we define the error variable as $e_1 = x_1 - x_{1,c}$, and the derivative of e_1 is obtained by:

$$\dot{e}_1 = \dot{x}_1 - \dot{x}_{1,c} = x_2 - \dot{x}_{1,c} + d_1 \tag{29}$$

Then, we introduce the virtual control $x_{2,d}$ as the following form:

$$x_{2,d} = -k_1 e_1 - \frac{e_0}{Q_c^2 - e_0^2} - \hat{d}_1 \tag{30}$$

where \hat{d}_1 denotes the estimation error of the uncertainties d_1 , and k_1 is a positive constant. Similarly, the filter is used as $\dot{x}_{2,c} = -\frac{x_{2,c} - x_{2,d}}{\tau_2} - \zeta_2 \tanh(c_2(x_{2,c} - x_{2,d}))$, $x_{2,c}(0) = x_{2,d}(0)$, where ζ_2, c_2, τ_2 are positive constants.

Next, we define the error variable as $e_2 = x_2 - x_{2,c}$, and the virtual control is designed as:

$$x_{3,d} = -k_2 e_2 - e_1 \tag{31}$$

Similarly, the filter is used as $\dot{x}_{3,c} = -\frac{x_{3,c} - x_{3,d}}{\tau_3} - \zeta_3 \tanh(c_3(x_{3,c} - x_{3,d}))$, $x_{3,c}(0) = x_{3,d}(0)$, where ζ_3, c_3, τ_3 are positive constants.

Finally, the controller is obtained by:

$$u = \frac{1}{b}(-a_3 x_2 - a_4 \hat{x}_3 - k_3 e_3 - e_2 - \hat{d}_3) \tag{32}$$

where the error variable is defined as $e_3 = \hat{x}_3 - x_{3,c}$, where \hat{x}_3 is estimated by the OFTDO. The term \hat{d}_3 denotes the estimation error of the uncertainties d_3 by the proposed OFTDO, and k_3 is a positive constant.

4.4. Stability Analysis

This part provides the stability analysis of the closed-loop system under the proposed IGC law (32).

Define that:

$$\bar{e}_3 = \hat{x}_3 - x_3, e_{f,i} = x_{i,c} - x_{i,d}, \tilde{d}_i = d_i - \hat{d}_i (i = 0, 1, 3) \tag{33}$$

where \bar{e}_3 denotes the estimation error of the state x_3 , and \tilde{d}_i represents the estimation error of the disturbance d_i and the filter error.

A Lyapunov function candidate is selected as:

$$V_0 = \frac{1}{2} \log\left(\frac{Q_c^2}{Q_c^2 - e_0^2}\right) \tag{34}$$

where log denotes the natural logarithm. Note that $x_1 - x_{1,d} = e_1 + e_{f,1}$ and taking the derivative of V_0 yields:

$$\begin{aligned}
 \dot{V}_0 &= \frac{Q_c^2 - e_0^2}{2Q_c^2} \frac{-Q_c^2}{(Q_c^2 - e_0^2)^2} (-2e_0\dot{e}_0) \\
 &= \frac{e_0\dot{e}_0}{Q_c^2 - e_0^2} \\
 &= -\frac{k_0e_0^2}{A_c^2 - e_0^2} - \frac{e_0^2}{2(Q_c^2 - e_0^2)^2} + \frac{e_0(x_1 - x_{1,d})}{Q_c^2 - e_0^2} + \frac{e_0\tilde{d}_0}{Q_c^2 - e_0^2} \\
 &= -\frac{k_0e_0^2}{A_c^2 - e_0^2} - \frac{e_0^2}{2(Q_c^2 - e_0^2)^2} + \frac{e_0(e_1 + e_{f,1})}{Q_c^2 - e_0^2} + \frac{e_0\tilde{d}_0}{Q_c^2 - e_0^2}
 \end{aligned} \tag{35}$$

Substituting (30) into (29) yields that:

$$\begin{aligned}
 \dot{e}_1 &= x_2 - \dot{x}_{1,c} + d_1 \\
 &= e_2 - \bar{e}_2 + e_{f,2} + x_{2,d} + d_1 - \dot{x}_{1,c} \\
 &= -k_1e_1 + e_2 + e_{f,2} - \frac{e_0}{Q_c^2 - e_0^2} + \tilde{d}_1 - \dot{x}_{1,c}
 \end{aligned} \tag{36}$$

Combining (31) and taking the derivative of e_2 yields that:

$$\begin{aligned}
 \dot{e}_2 &= \dot{x}_2 - \dot{x}_{2,c} \\
 &= x_3 - \dot{x}_{2,c} \\
 &= e_3 - \bar{e}_3 + e_{f,3} + x_{3,d} - \dot{x}_{2,c} \\
 &= -k_2e_2 + e_3 - \bar{e}_3 + e_{f,3} - e_1 - \dot{x}_{2,c}
 \end{aligned} \tag{37}$$

Calculating the derivative of e_3 and substituting the controller (32), one has that:

$$\begin{aligned}
 \dot{e}_3 &= \dot{x}_3 - \dot{x}_{3,c} \\
 &= a_3x_2 + a_4x_3 + bu - \dot{x}_{3,c} + d_3 + \dot{\bar{e}}_3 \\
 &= -a_4\bar{e}_3 - k_3e_3 - e_2 + \tilde{d}_3 - \dot{x}_{3,c} + \dot{\bar{e}}_3
 \end{aligned} \tag{38}$$

We choose a new Lyapunov function as:

$$V = V_0 + \frac{1}{2} \sum_{i=1}^3 e_i^2 + \frac{1}{2} \sum_{i=1}^3 e_{f,i}^2 + \frac{1}{2} \bar{e}_3^2 \tag{39}$$

Note that:

$$\dot{e}_{f,i} = -\frac{e_{f,i}}{\tau_i} - \zeta_i \tanh(c_i e_{f,i}) - \dot{x}_{i,d} \tag{40}$$

and taking the derivative of V yields:

$$\begin{aligned}
 \dot{V} &= \dot{V}_0 + \sum_{i=1}^3 \dot{e}_i e_i + \sum_{i=1}^3 \dot{e}_{f,i} e_{f,i} + \dot{\bar{e}}_3 \bar{e}_3 \\
 &= -\frac{k_0e_0^2}{Q_c^2 - e_0^2} - \frac{e_0^2}{2(Q_c^2 - e_0^2)^2} + \frac{e_0(e_1 + e_{f,1})}{Q_c^2 - e_0^2} + \frac{e_0\tilde{d}_0}{Q_c^2 - e_0^2} \\
 &\quad - k_1e_1^2 + e_1e_2 + e_1e_{f,2} - \frac{e_1e_0}{Q_c^2 - e_0^2} + e_1\tilde{d}_1 - e_1\dot{x}_{1,c} \\
 &\quad - k_2e_2^2 + e_2e_3 - e_2\bar{e}_3 + e_2e_{f,3} - e_2e_1 - e_2\dot{x}_{2,c} \\
 &\quad - k_3e_3^2 - a_4e_3\bar{e}_3 - e_3e_2 + e_3\tilde{d}_3 - e_3\dot{x}_{3,i} + e_3\dot{\bar{e}}_3 \\
 &\quad + \sum_{i=1}^3 \left(-\frac{e_{f,i}^2}{\tau_i} - \zeta_i e_{f,i} \tanh(c_i e_{f,i}) - e_{f,i} \dot{x}_{i,d} \right) + \dot{\bar{e}}_3 \bar{e}_3
 \end{aligned} \tag{41}$$

Reorganizing the derivative of V yields that:

$$\begin{aligned} \dot{V} = & -\frac{k_0 e_0^2}{Q_c^2 - e_0^2} - \sum_{i=1}^3 k_i e_i^2 - e_2 \bar{e}_3 - a_4 e_3 \bar{e}_3 \\ & - \frac{e_0^2}{2(Q_c^2 - e_0^2)^2} + \frac{e_0 e_{f,1}}{Q_c^2 - e_0^2} + e_1 e_{f,2} + e_2 e_{f,3} \\ & + \frac{e_0 \tilde{d}_0}{Q_c^2 - e_0^2} + e_1 \tilde{d}_1 + e_3 \tilde{d}_3 - e_1 \dot{x}_{1,c} - e_2 \dot{x}_{2,c} - e_3 \dot{x}_{3,c} + 2\dot{\bar{e}}_3 \bar{e}_3 \\ & + \sum_{i=1}^3 \left(-\frac{e_{f,i}^2}{\tau_i} - \zeta_i e_{f,i} \tanh(c_i e_{f,i}) - e_{f,i} \dot{x}_{i,d} \right) \end{aligned} \tag{42}$$

Utilizing Young’s inequality, the following relationships are satisfied:

$$\frac{e_0 e_{f,1}}{Q_c^2 - e_0^2} \leq \frac{e_0^2}{4(Q_c^2 - e_0^2)^2} + e_{f,1}^2, \quad e_1 e_{f,2} \leq \frac{e_1^2}{4} + e_{f,2}^2, \quad e_2 e_{f,3} \leq \frac{e_2^2}{4} + e_{f,3}^2 \tag{43}$$

$$-e_2 \bar{e}_3 \leq e_2^2 + \frac{\bar{e}_3^2}{4} \tag{44}$$

$$\frac{e_0 \tilde{d}_0}{Q_c^2 - e_0^2} \leq \frac{e_0^2}{4(Q_c^2 - e_0^2)^2} + \tilde{d}_0^2, \quad e_i \tilde{d}_i \leq \frac{e_i^2}{4} + \tilde{d}_i^2 \tag{45}$$

$$-\zeta_i e_{f,i} \tanh(c_i e_{f,i}) \leq -\zeta_i |e_{f,i}| + \frac{\zeta_i k_p}{c_i} \tag{46}$$

$$-e_{f,i} \dot{x}_{i,d} \leq \frac{e_{f,i}^2}{2} + \frac{\dot{x}_{i,d}^2}{2} \quad (i = 1, 2, 3) \tag{47}$$

and substituting (43)–(47) into (42) yields:

$$\begin{aligned} \dot{V} = & -\frac{k_0 e_0^2}{Q_c^2 - e_0^2} - (k_1 - \frac{3}{2})e_1^2 - (k_2 - \frac{3}{2})e_2^2 - (k_3 - \frac{9}{4})e_3^2 + \sum_{i=1}^3 \left((\frac{3}{2} - \frac{1}{\tau_i})e_{f,i}^2 - \zeta_i |e_{f,i}| \right) \\ & + \sum_{i=0}^3 \tilde{d}_i + \frac{1+a_4^2}{4}\bar{e}_3^2 + \sum_{i=1}^3 \frac{\dot{x}_{i,d}}{2} + \sum_{i=1}^3 \frac{\zeta_i k_p}{c_i} + 2\dot{\bar{e}}_3 \bar{e}_3 \end{aligned} \tag{48}$$

According to Lemma 3, one has that:

$$\begin{aligned} \dot{V} \leq & -k_0 \log\left(\frac{Q_c^2}{Q_c^2 - e_0^2}\right) - (k_1 - \frac{3}{2})e_1^2 - (k_2 - \frac{3}{2})e_2^2 - (k_3 - \frac{9}{4})e_3^2 \\ & + \sum_{i=1}^3 \frac{5\tau_i - 1}{\tau_i} e_{f,i}^2 + \frac{1+a_4^2}{4}\bar{e}_3^2 + M \end{aligned} \tag{49}$$

where $M = \tilde{d}_0 + \tilde{d}_1 + \tilde{d}_3 + \sum_{i=1}^3 \frac{\dot{x}_{i,d}}{2} + \sum_{i=1}^3 \frac{\zeta_i}{4} + \sum_{i=1}^3 \frac{\zeta_i k_p}{c_i} + 2\dot{\bar{e}}_3 \bar{e}_3$. Note that the estimation of the states and uncertainties are achieved in finite time, and thus $\hat{x}_3 = x_3$ and $\hat{d}_i = d_i$ ($i = 0, 1, 3$) hold after a finite time moment t_f . Assume that the term $\dot{x}_{i,d}$ is also bounded; then we have $M \leq \bar{M}$, in which \bar{M} is a positive constant. Therefore, one has:

$$\dot{V} \leq -2\mu V + \bar{M} \tag{50}$$

where $\mu = \min\{k_0, k_1 - \frac{3}{2}, k_2 - \frac{3}{2}, k_3 - \frac{9}{4}, \frac{5\tau_i - 1}{\tau_i}, \frac{1+a_4^2}{4}\}$. Then, the following theorem is obtained.

Theorem 2. Consider the IGC system (11). If the controller is designed as (26), (30), (31) and (32), the initial value satisfies $|q_b(0)| < Q_c$, and $k_i, \tau_i (i = 1, 2, 3)$ are chosen such as $\mu > 0$, then the system will have the following properties:

- (a) The tracking errors of the system state are ultimately bounded.
- (b) The constraint requirement $|q_b| < Q_c$ will not be violated.

Proof. Integrating (50), we obtain:

$$V \leq (V(0) - \frac{\bar{M}}{2\mu})e^{-2\mu t} + \frac{\bar{M}}{2\mu} \tag{51}$$

therefore, the function V is bounded, which implies that all of the states of the closed-loop system are bounded, and the tracking errors are ultimately bounded.

Moreover, from (39) and (50), we can conclude that $|e_0| < Q_c$ holds if the initial value satisfies $|e_0| < Q_c$ according to Lemma 1. Therefore, the constraint requirement is not violated during the dynamic process. The proof is completed.

Remark 5. It is worth noting that the estimation errors \bar{e}_i and \bar{d}_i will converge to zero in finite time by the proposed OFTDO. Therefore, the convergence boundary \bar{M} is only related to the terms $\sum_{i=1}^3 \frac{\hat{x}_{i,d}}{2}, \sum_{i=1}^3 \frac{\hat{\xi}_i}{4}$ and $\sum_{i=1}^3 \frac{\hat{\xi}_i k_p}{c_i}$. If c_i is selected to be large enough, we have $\frac{\hat{\xi}_i k_p}{c_i} \rightarrow 0$. If the command $\hat{\xi}_i$ is chosen to be small, the final convergence domain will be decreased.

The schematic diagram of the proposed control scheme is provided in Figure 3. As shown in Figure 3, the presented approach achieves a control framework that covers the FOV requirement, partial measurement and unmatched uncertainties.

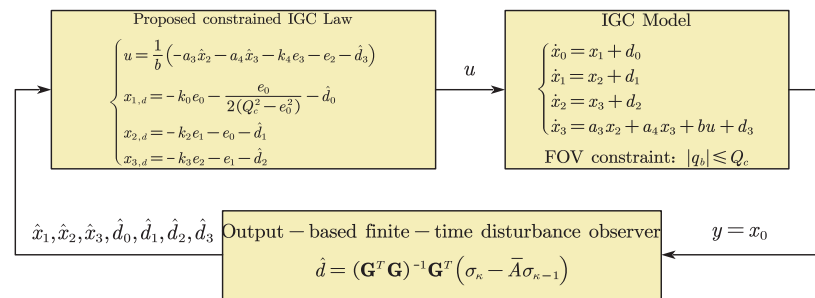


Figure 3. Schematic diagram of the proposed control.

5. Simulation and Discussion

5.1. Simulation Settings

The initial conditions were set as $R = 60$ km and $z_m = 27$ km, and the location of the target was set as $x_T = 53$ km and $z_T = 0$. The initial angles of the hypersonic flight vehicle were $\alpha(0) = 0.1^\circ$, $\omega_z(0) = 0.1^\circ/s$. The missile and the target were set to fly with constant velocities of 6 Ma and 0 m/s, respectively. The aerodynamic coefficients were set as:

$$a_1 = \frac{57.3QS c_y^\alpha}{mV_M} = 0.3487, a_2 = \frac{57.3QS c_y^{\delta_z}}{mV_M} = 0.068, a_3 = \frac{57.3QSLm_z^\alpha}{J_z} = -17.801$$

$$a_4 = \frac{57.3QSL^2 m_z^{\omega_z}}{J_z V_M} = -0.2741, b = \frac{57.3QSLm_z^{\delta_z}}{J_z} = -31.267 \tag{52}$$

The control input was restricted as $|u| \leq 25$ deg. The FOV constraint was set as $Q_c = 12^\circ$. Parameters of the proposed control method were chosen as $k_1 = 1, k_2 = 2, r_3 = 1, \tau_1 = \tau_2 = \tau_3 = 0.1, \xi_1 = \xi_2 = \xi_3 = 0.5, c_1 = c_2 = c_3 = 2$.

5.2. Results and Discussions

The simulation results are shown in Figures 4–10 and the estimations of the disturbances are shown in Figures 11–13. As seen in Figures 4 and 5, the final miss of distance is small, which means that the fine engagement has been achieved by the proposed IGC law $u = \frac{1}{b}(-a_3x_2 - a_4\hat{x}_3 - k_3e_3 - e_2 - \hat{d}_3)$ in (32). Moreover, the BLOS angle q_b is constrained in the prescribed FOV limitations, which shows that the FOV constraint Q_c is not violated in the flight procedure. The angle of attack α , pitch rate ω_z and evaluator δ_z are shown in Figures 8–10. Meanwhile, the estimation d_0, d_1, d_3 of the uncertainties in Figures 11–13 demonstrates that the proposed OFTDO has achieved the finite-time estimation of the unknown unmatched uncertainties successfully.

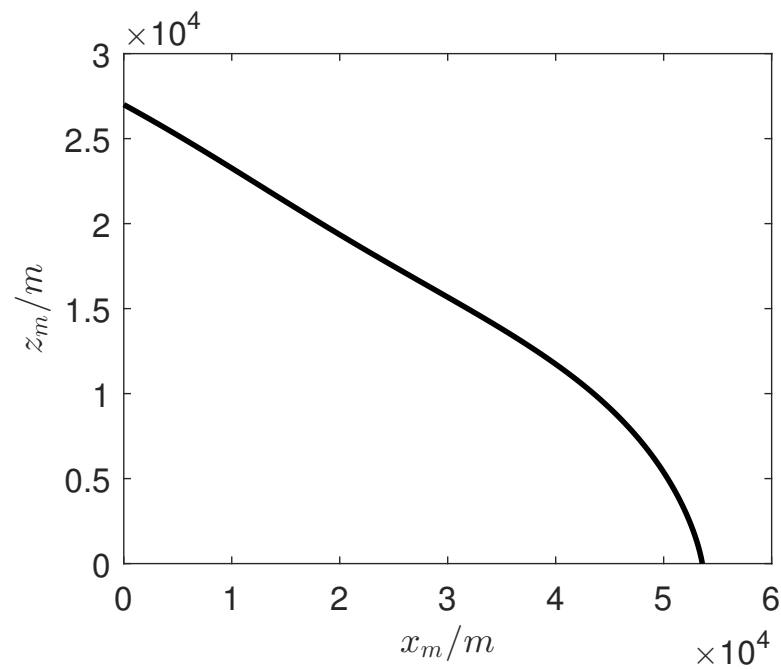


Figure 4. Curve of trajectory on the x and z axes.

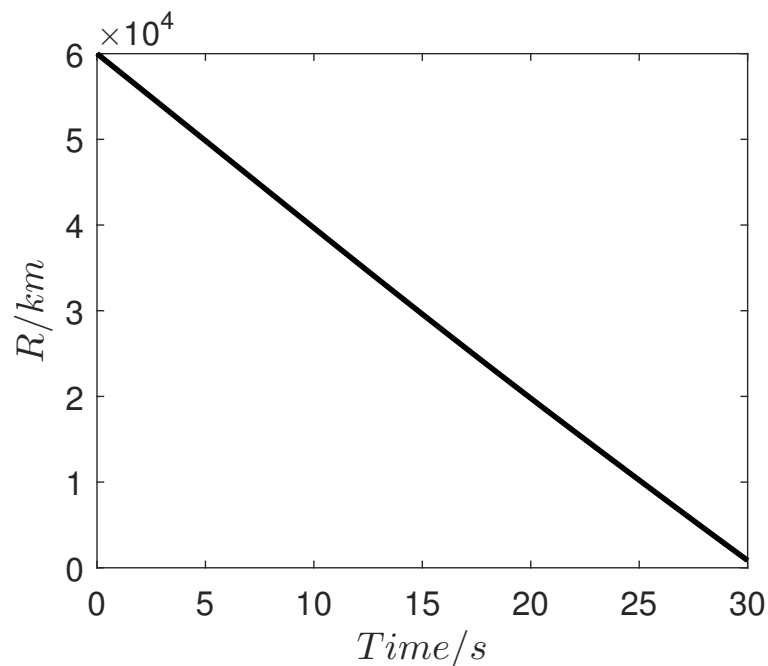


Figure 5. Curve of the relative distance R .

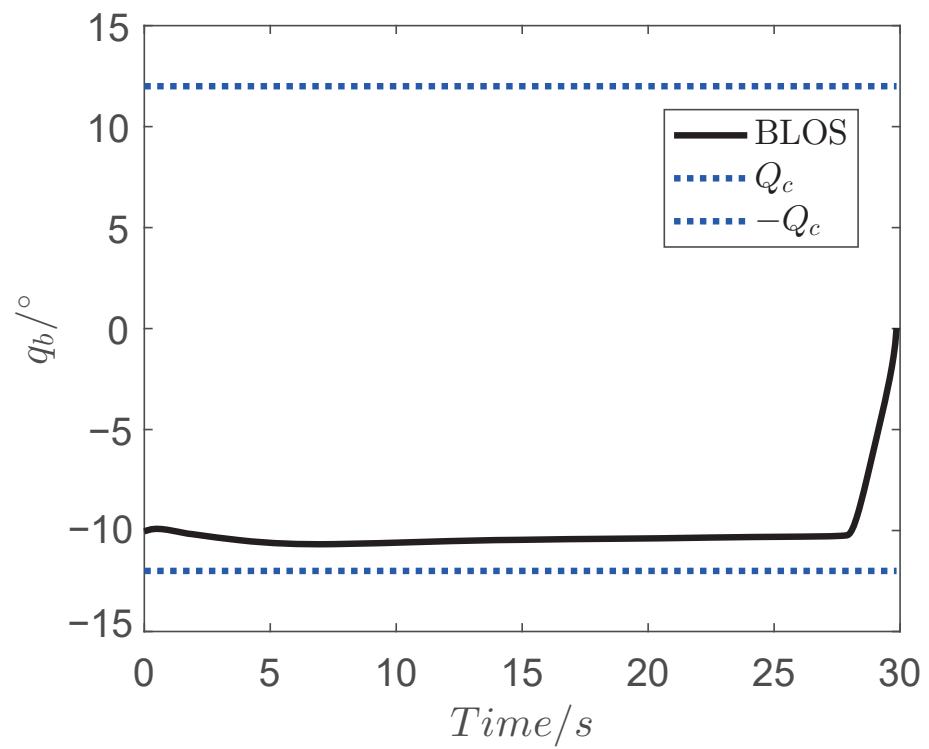


Figure 6. Curve of body line-of-sight angle q_b .

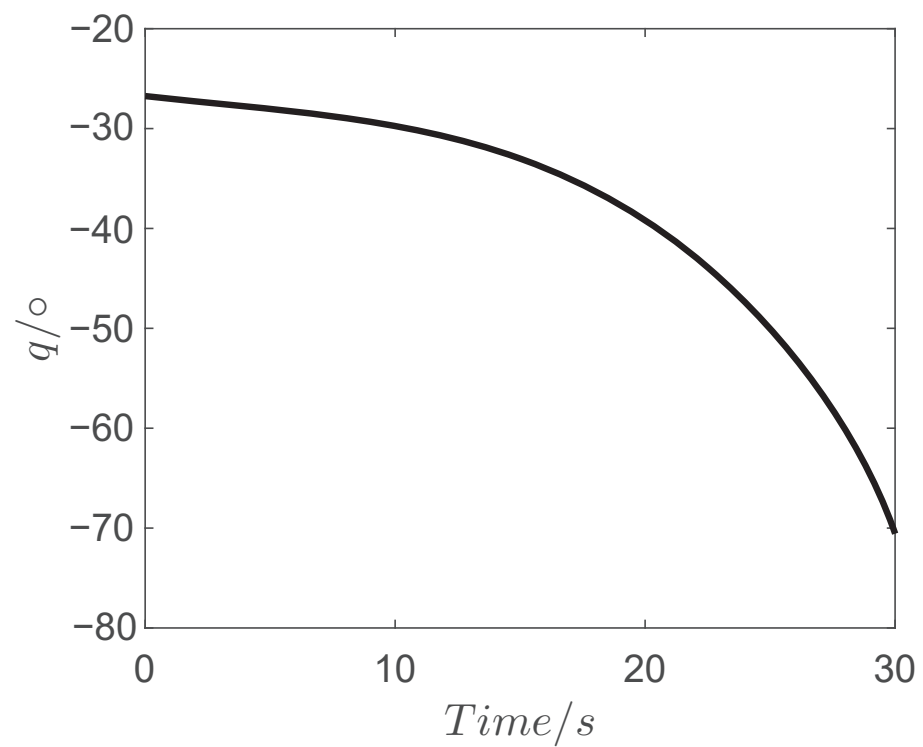


Figure 7. Curve of line-of-sight angle q .

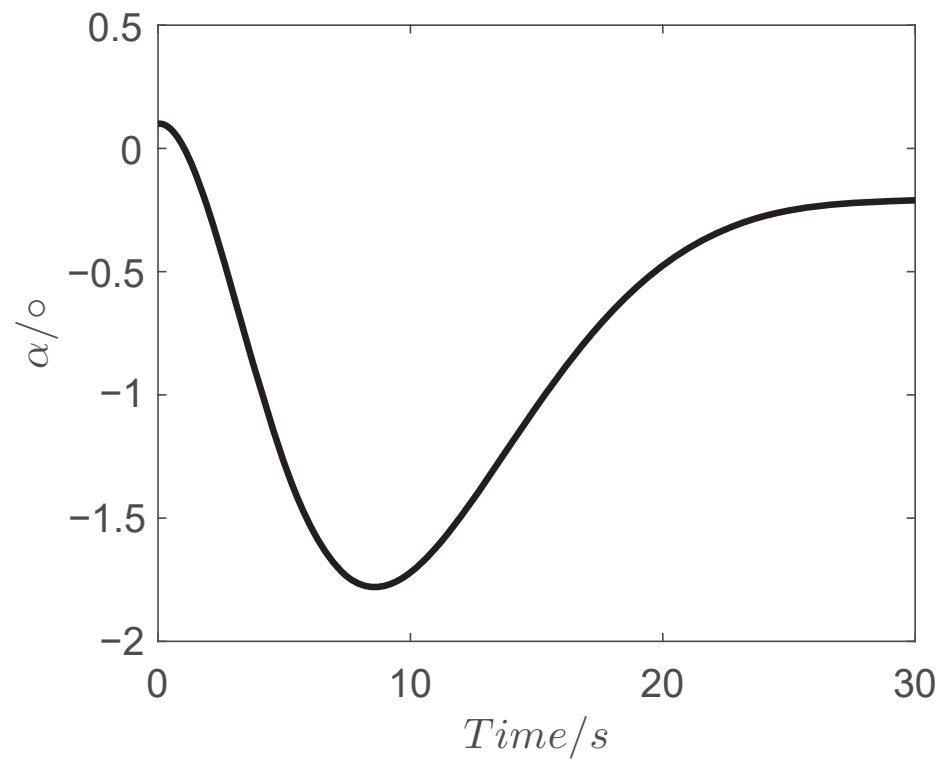


Figure 8. Curve of the angle of attack α .

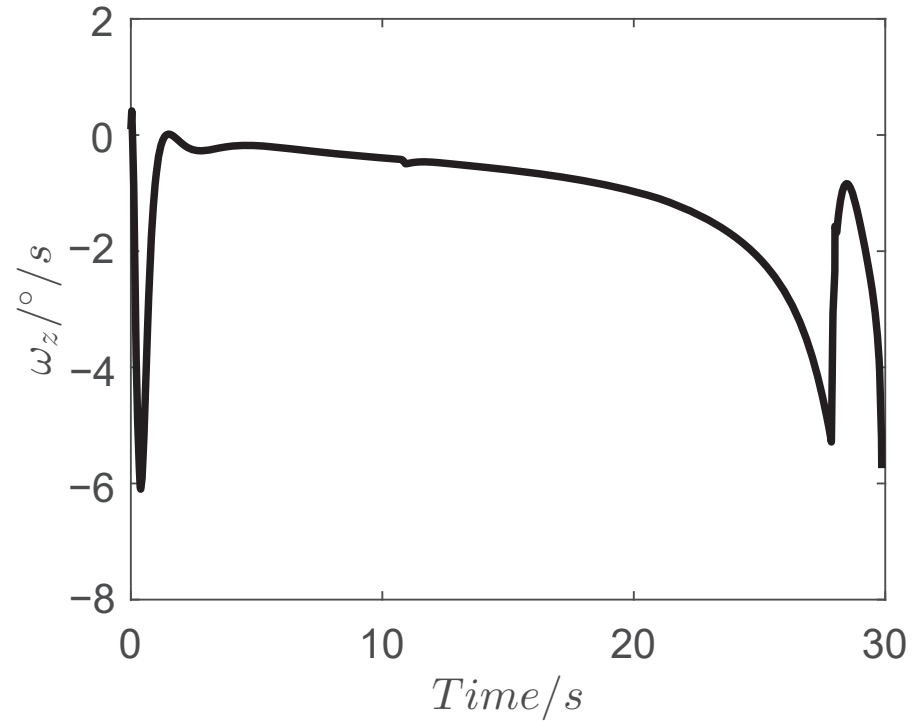


Figure 9. Curve of the pitch rate ω_z .

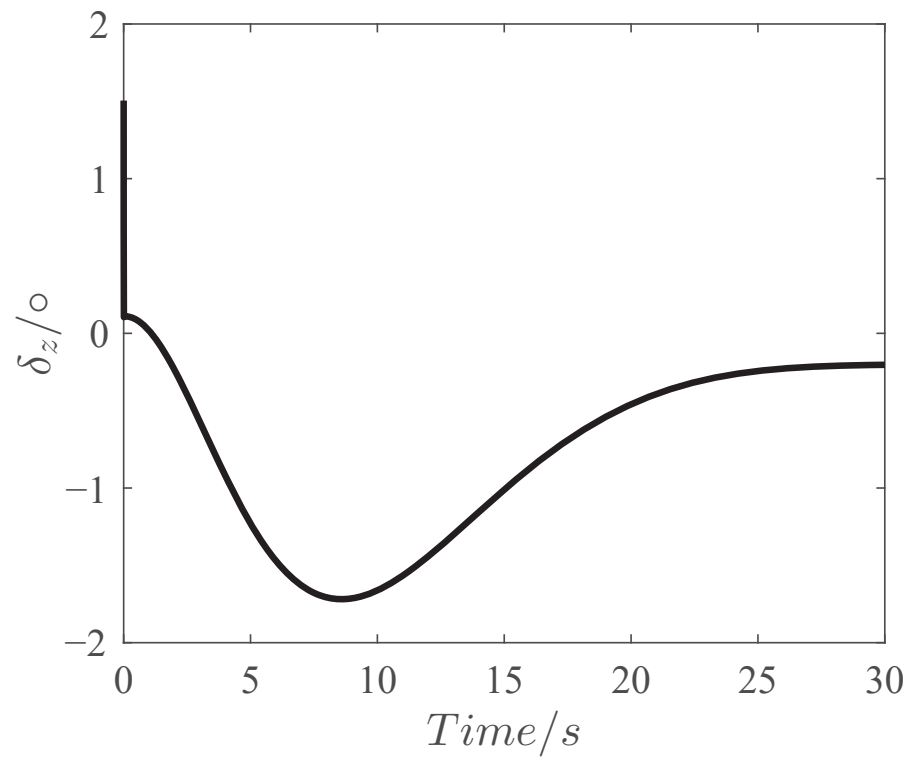


Figure 10. Curve of the elevator δ_z .

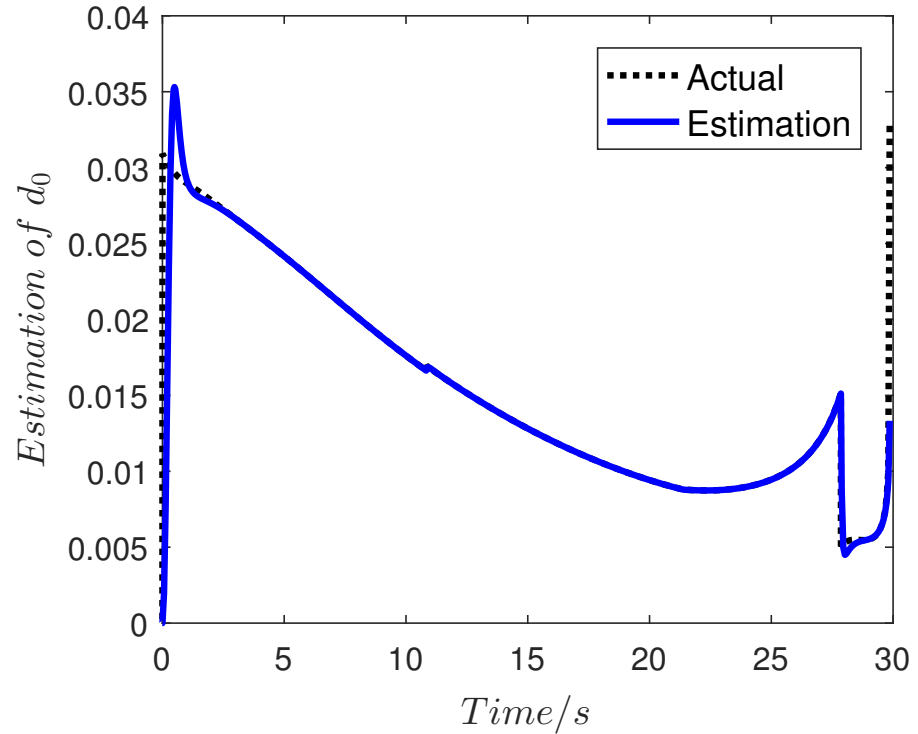


Figure 11. Curve of the estimation d_0 .

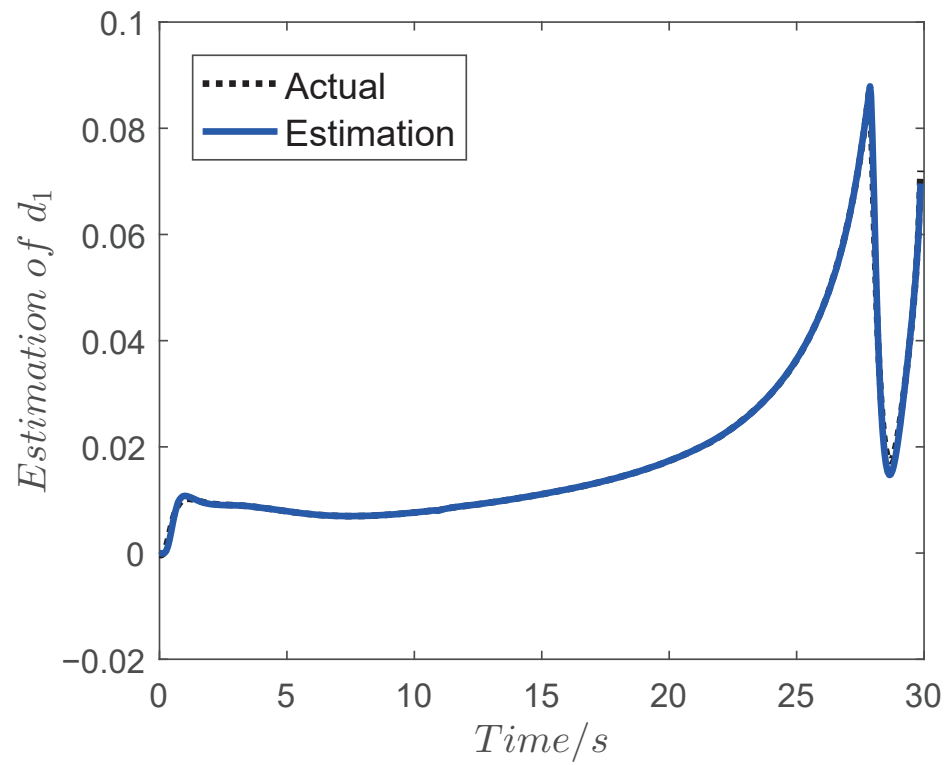


Figure 12. Curve of the estimation d_1 .

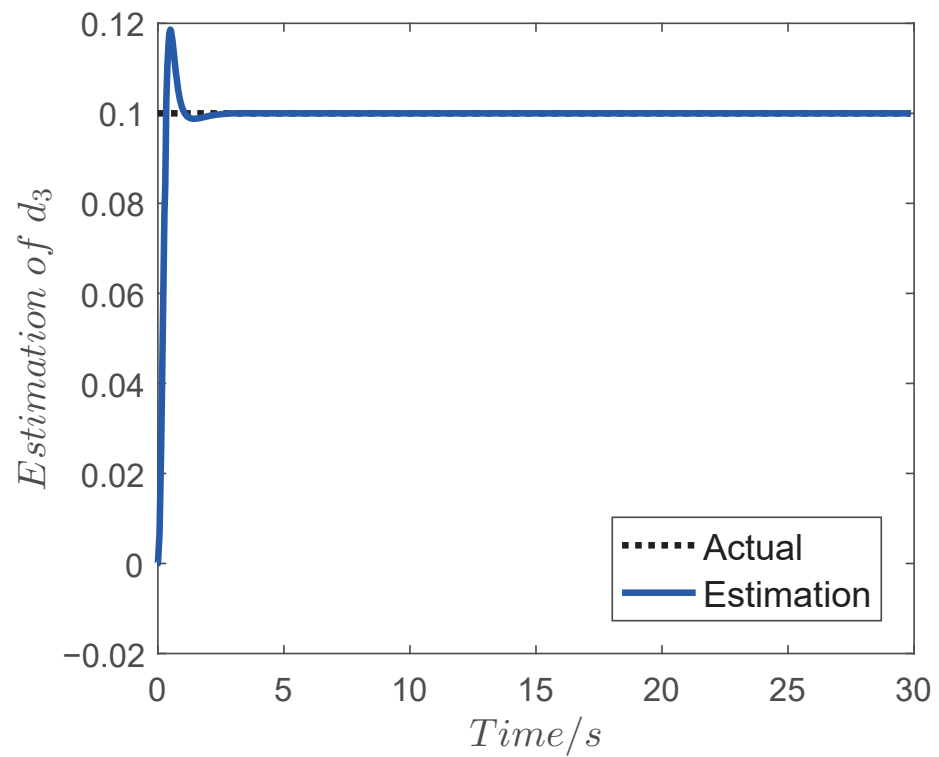


Figure 13. Curve of the estimation d_3 .

To further test the robustness and effectiveness of the proposed IGC law, Monte-Carlo tests were carried out in the simulation. The number of the tests was set as 500 times, and the final location on the x and z axes and the missed distance are shown in Figures 14 and 15, respectively. The mean and the standard deviation can be calculated as 0.501 m and 0.7741 m, respectively. As seen in these figures, the distribution of the missed distance is smaller than 1 m, which shows the strong robustness of the proposed IGC law.

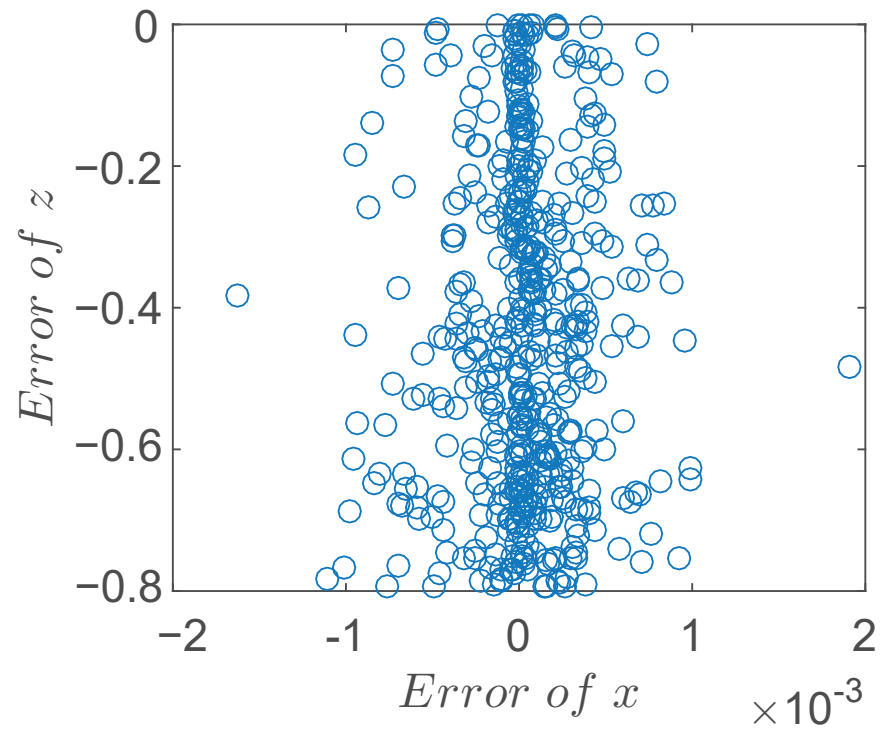


Figure 14. Curve of Monte-Carlo results on the x and z axes.

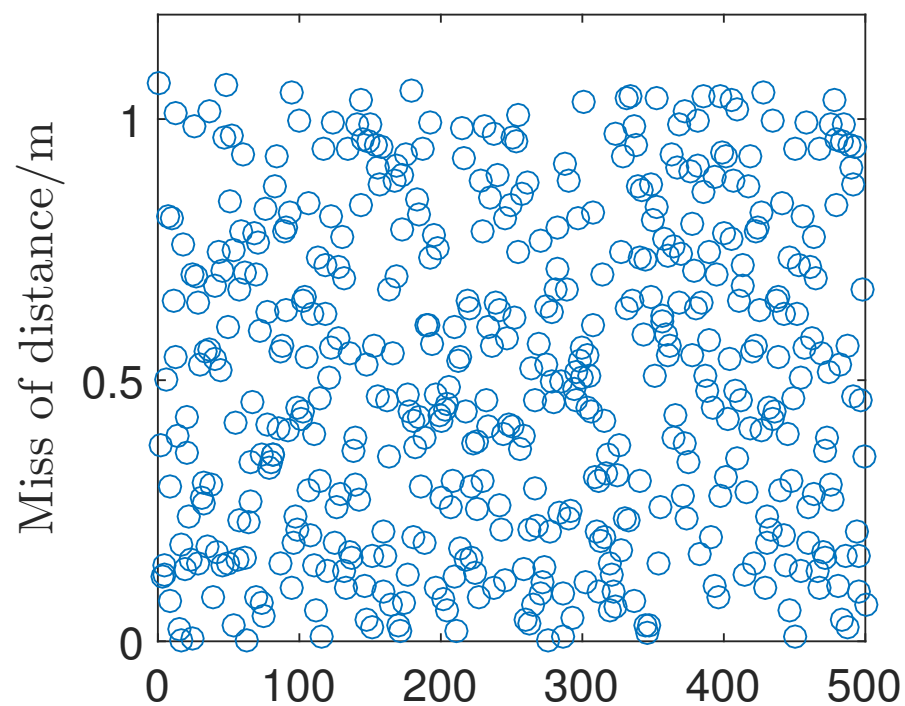


Figure 15. Curve of the missed distance in the Monte-Carlo tests.

6. Conclusions

An integrated guidance and control law for strap-down hypersonic flight vehicles was proposed, with partial measurement information and unmatched uncertainties. A constrained IGC scheme was proposed by combining the barrier Lyapunov function-based backstepping methodology and the specific output-based finite-time disturbance observer. The effectiveness of the presented scheme was verified by numerical simulations and Monte-Carlo tests. Future researches include the the constrained performance optimization, and consideration of the actuator dynamics and wind gust disturbance.

Author Contributions: Methodology, M.D.; software, X.X. and F.X.; writing—original draft preparation, M.D.; writing—review and editing, M.D. All authors have read and agreed to the published version of the manuscript.

Funding: This research received no external funding.

Institutional Review Board Statement: Not applicable.

Informed Consent Statement: Not applicable.

Data Availability Statement: Not applicable.

Conflicts of Interest: The authors declare no conflict of interest.

References

1. Bolender, M.A. An overview on dynamics and controls modelling of hypersonic vehicles. In Proceedings of the 2009 American Control Conference, St. Louis, MO, USA, 10–12 June 2009; pp. 2507–2512.
2. Fiorentini, L.; Serrani, A. Adaptive restricted trajectory tracking for a non-minimum phase hypersonic vehicle model. *Automatica* **2012**, *48*, 1248–1261. [[CrossRef](#)]
3. Lv, M.; Schutter, B.; Baldi, S. Non-Recursive Control for Formation-Containment of HFV Swarms with Dynamic Event-Triggered Communication. *IEEE Trans. Ind. Informat.* **2022**. [[CrossRef](#)]
4. Sagliano, M.; Mooij, E.; Theil, S. Adaptive disturbance-based high-order sliding-mode control for hypersonic-entry vehicle. *J. Guid. Control Dyn.* **2017**, *40*, 521–536. [[CrossRef](#)]
5. Guo, Z.Y.; Guo, J.G.; Zhou, J.; Chang, J. Robust tracking for hypersonic reentry vehicles via disturbance estimation-triggered control. *IEEE Trans. Aerosp. Electron. Syst.* **2019**, *56*, 1279–1289. [[CrossRef](#)]
6. Zong, Q.; Ji, Y.; Zeng, F.; Liu, H. Output feedback back-stepping control for a generic hypersonic vehicle via small-gain theorem. *Aerosp. Sci. Technol.* **2012**, *23*, 409–417. [[CrossRef](#)]
7. Hu, G.J.; Guo, J.G.; Guo, Z.Y.; Cieslak, J.; Henry, D. ADP-based intelligent tracking algorithm for reentry vehicles subjected to model and state uncertainties. *IEEE Trans. Ind. Informat.* **2022**. [[CrossRef](#)]
8. Xiong, Z.; Peng, H.; Wang, J.; Wang, R.; Liu, J.Y. Dynamic calibration method for SINS lever-arm effect for HCVs. *IEEE Trans. Aerosp. Electron. Syst.* **2015**, *51*, 2760–2771. [[CrossRef](#)]
9. Chen, K.; Zhou, J.; Shen, F.Q.; Sun, H.Y.; Fan, H. Hypersonic boost-glide vehicle strap-down inertial navigation system/global positioning system algorithm in a launch-centered earth-fixed frame. *Aerosp. Sci. Technol.* **2020**, *98*, 105679. [[CrossRef](#)]
10. Wang, J.H.; Liu, L.H.; Zhao, T.; Tang, G.J. Integrated guidance and control for hypersonic vehicles in dive phase with multiple constraints. *Aerosp. Sci. Technol.* **2016**, *53*, 103–116. [[CrossRef](#)]
11. Koren, A.; Idan, M.; Golan, O.M. Integrated sliding mode guidance and control for a missile with on-off actuators. *J. Guid. Control Dyn.* **2008**, *31*, 204–214. [[CrossRef](#)]
12. Guo, J.G.; Xiong, Y.; Zhou, J. A new sliding mode control design for integrated missile guidance and control system. *Aerosp. Sci. Technol.* **2018**, *78*, 54–61. [[CrossRef](#)]
13. Panchal, B.; Mate, N.; Talole, S.E. Continuous-time predictive control-based integrated guidance and control. *J. Guid. Control Dyn.* **2017**, *40*, 1579–1595. [[CrossRef](#)]
14. Santoso, F.; Garratt, M.A.; Anavatti, S.G. State-of-the-art integrated guidance and control systems in unmanned vehicles: A Review. *IEEE Syst. J.* **2021**, *15*, 3312–3323. [[CrossRef](#)]
15. Tee, K.P.; Ge, S.S.; Tay, E.H. Barrier Lyapunov functions for the control of output-constrained nonlinear systems. *Automatica* **2009**, *45*, 918–927. [[CrossRef](#)]
16. Ren, B.; Ge, S.S.; Tee, K.P.; Lee, T.H. Adaptive neural control for output feedback nonlinear systems using a barrier Lyapunov function. *IEEE Trans. Neural Netw.* **2010**, *21*, 1339–1345.
17. Lv, M.; Chen, Z.; Schutter, B.; Baldi, S. Prescribed-performance tracking for high-power nonlinear dynamics with time-varying unknown control coefficients. *Automatica* **2022**, *146*, 110584. [[CrossRef](#)]
18. Guo, Z.; Henty, D.; Guo, J.; Wang, Z.; Cieslak, J.; Chang, J. Control for systems with prescribed performance guarantees: An alternative interval theory-based approach. *Automatica* **2022**, *146*, 110642. [[CrossRef](#)]

19. Li, P.; Yang, G.H. Fault-tolerant control of uncertain nonlinear systems with nonlinearly parameterized fuzzy systems. In Proceedings of the 2009 IEEE Control Applications, (CCA) & Intelligent Control, (ISIC), St. Petersburg, Russia, 8–10 July 2009; pp. 382–387.
20. Flores, G.; Oca, A.; Flores, A. Robust Nonlinear Control for the Fully Actuated Hexa-Rotor: Theory and Experiments. *IEEE Control Syst. Lett.* **2023**, *7*, 277–282. [[CrossRef](#)]
21. Guan, Z.; Liu, H.; Zheng, Z.; Ma, Y.; Zhu, T. Moving path following with integrated direct lift control for carrier landing. *Aerospace Sci. Technol.* **2022**, *120*, 107247. [[CrossRef](#)]
22. Ohishi, K.; Nakao, M.; Ohnishi, K.; Miyachi, K. Microprocessor-controlled dc motor for load-insensitive position servo system. *IEEE Trans. Ind. Electron.* **1987**, *IE-34*, 44–49. [[CrossRef](#)]
23. Chen, W.H.; Ohnishi, K.; Guo, L. Advances in disturbance/uncertainty estimation and attenuation. *IEEE Trans. Ind. Electron.* **2015**, *62*, 5758–5762. [[CrossRef](#)]
24. Han, J. Extended state observer for a class of uncertain plants (in Chinese). *Control Decis.* **1995**, *10*, 85–88.
25. Chen, W.H.; Yang, J.; Guo, L.; Li, S.H. Disturbance-observer-based control and related methods—An overview. *IEEE Trans. Ind. Electron.* **2016**, *63*, 1083–1095. [[CrossRef](#)]
26. Wang, P.; Zhang, X.B.; Zhu, J.H. Integrated Missile Guidance and Control: A Novel Explicit Reference Governor Using a Disturbance Observer. *IEEE Trans. Ind. Electron.* **2019**, *66*, 5487–5496. [[CrossRef](#)]
27. Dong, W.J.; Farrell, J.A.; Polycarpou, M.M.; Djapic, V.; Sharma, V. Command filtered adaptive backstepping. *IEEE Trans. Control Syst. Technol.* **2012**, *20*, 566–580. [[CrossRef](#)]
28. Yang, J.; Li, S.; Sun, C.; Guo, L. Nonlinear disturbance observer based robust flight control for airbreathing hypersonic vehicles. *IEEE Trans. Aerosp. Electron. Syst.* **2013**, *49*, 1263–1275. [[CrossRef](#)]
29. Kratz, W. Characterization of strong observability and construction of an observer. *Linear Algebra Its Appl.* **1995**, *221*, 31–40. [[CrossRef](#)]
30. Levant, A. Higher-order sliding modes, differentiation and output-feedback control. *Int. J. Control* **2003**, *76*, 924–941. [[CrossRef](#)]
31. Ferreira, A.; Cieslak, J.; Henry, D.; Zolghadri, A.; Fridman, L. Output tracking of systems subjected to perturbations and a class of actuator faults based on HOSM observation and identification. *Automatica* **2015**, *59*, 200–205. [[CrossRef](#)]
32. Ferreira, A.; Bejarano, F.; Fridman, L. Robust Control With Exact Uncertainties Compensation: With or Without Chattering? *IEEE Trans. Control Syst. Technol.* **2011**, *19*, 969–975. [[CrossRef](#)]